Engineering Structures 281 (2023) 115748

Contents lists available at ScienceDirect

Engineering Structures

journal homepage: www.elsevier.com/locate/engstruct

Shaking table experimental investigations on dynamic characteristics of CFRP cable dome

Weihong Qin [a,b], Han Gao [a,b], Zhuo Xi [a,b,*], Peng Feng [c], Yunjie Li [a,b]

[a] Key Laboratory of Concrete and Prestressed Concrete Structures of Ministry of Education, Nanjing 211189, China
[b] National Prestress Engineering Research Center, Southeast University, Nanjing 211189, China
[c] School of Civil Engineering, Tsinghua University, Beijing 100084, China

ARTICLE INFO

Keywords:
Shaking table test
Cable dome
Carbon fiber reinforced polymer
Seismic performance

ABSTRACT

Carbon fiber reinforced polymer (CFRP) bars have the feature of lower density, higher strength and better anti-fatigue performance compared with steel bars. Therefore, CFRP is a kind of ideal material for a long-span spatial structure. To explore the dynamic performance of spatial structures and take full advantages of CFRP bars in long span cable dome structures, a CFRP cable dome scale model with a diameter of 5.4 m was designed for a shaking table test. In this model, struts and cables were made of CFRP material except that the internal ring beams were fabricated with steel. In the test, new types of joint forms and anchoring configurations for CFRP cable dome structures were proposed because the existing forms for steel domes cannot be applied to CFRP dome structures. In addition, three kinds of seismic waves including Elcentro wave, Kobe wave and Pasadena wave were selected to generate 12 load cases and the maximum acceleration was 900 Gal. The acceleration and strain response of the model under different types of seismic waves was researched. It is demonstrated that middle-ring upper joints have the largest acceleration response because the control vibration modes of the CFRP cable dome structure are anti-symmetric mode. In addition, a CFRP dome numerical model was established to carry out modal analysis by program ANSYS. By comparing the results of finite element modal analysis with the measured frequencies, the natural vibration modes of the structure are analyzed. Based on the results of seismic wave spectrum analysis and structural modal analysis, the Pasadena wave, which has a wide low frequency region for high Fourier amplitude, can excite the greatest acceleration response.

1. Introduction

The cable dome structure was first proposed by Geiger and applied into the Gymnastics Arena and the Fencing Arena in Seoul. Due to their high structural efficiency [1], beautiful appearance, long span [2], great bearing capacity [3] and light self-weight [4], cable domes have become popular as roofs of structures including arenas, stadiums and sport centers over the past few decades. With the increase of requirements for spatial structures and the development of various new materials, the trend of combining new kinds of materials with different structures is inevitable. Composite materials have the advantages of lightweight [5], corrosion resistance and high strength [6]. Among them, carbon fiber reinforced polymer (CFRP) provides outstanding fatigue behavior [7], excellent corrosion resistance, low coefficient of thermal expansion and convenience of construction [89]. Therefore, replacing steel cables with CFRP cables in practical engineering can save the investment of structural maintenance in the life cycle and enlarge the span of a structure [10].

In order to prove the feasibility of combining FRP cables with long-span structures and study the mechanical property of CFRP structures, CFRP cables were first applied to bridge structures. Wen et al. [11] carried out a numerical comparative study on a composite cable-stayed bridge with CFRP stay cables and CFRP bridge decks from a mechanical-behavior viewpoint. It was demonstrated that the use of CFRP stay cables and CFRP bridge decks in super long-span cable-stayed bridges was feasible and these types of composite cable-stayed bridges could become an excellent alternative to steel cable-stayed bridges. Yang et al. [12] researched the mechanical behavior of suspension bridges with various fiber-reinforced polymer (FRP) and hybrid FRP cables by the finite-element method. The results indicated that the application of FRP cables in long-span suspension bridges benefited the spanning ability, improved the load-carrying efficiency, and reduced the axial force of the

* Corresponding author.
E-mail addresses: qinweihong@seu.edu.cn (W. Qin), 220201226@seu.edu.cn (H. Gao), xizhuoxian@seu.edu.cn (Z. Xi), fengpeng@tsinghua.edu.cn (P. Feng).

https://doi.org/10.1016/j.engstruct.2023.115748
Received 6 July 2022; Received in revised form 19 November 2022; Accepted 30 January 2023
Available online 17 February 2023
0141-0296/

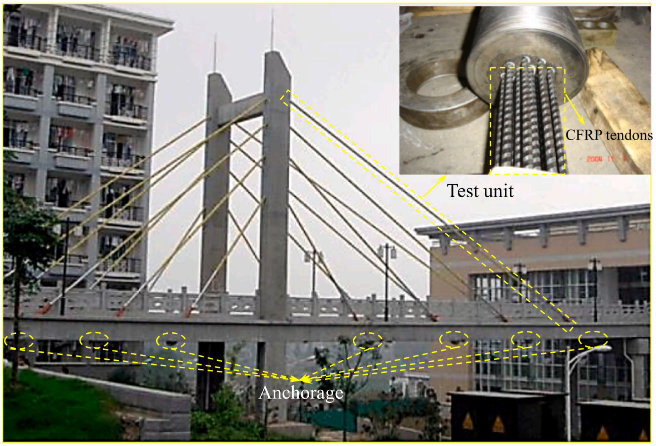

Fig. 1. The first CFRP cable stayed pedestrian bridge in Jiangsu University, China.

cable. Liu et al. [13] studied the parameter sensibility of a suspension bridge structural system with CFRP main cables through a fine finite element structural simulation. Moreover, the influence of structural parameters on the static and dynamic performance of long span suspension bridges was analyzed.

Besides, several experiments have been carried out to investigate static mechanical property of CFRP long-span bridge structures. In 1996, a cable-stayed pylon bridge of 124 m length was built in Winterthur, Switzerland in which CFRP cables were researched experimentally for the first time [14]. To test the tensile strength and installation techniques of CFRP cables, the first anchorage test (Fig. 1) for a cable-stayed bridge with CFRP cables in China was carried out in 2005 [15].

The above papers focus on bridge structures. In terms of spatial structures, Serdjuks et al. [16] studied geometrical characteristics of a saddle-shaped cable roof formed by CFRP load-carrying and contour cables and steel stabilizing cables numerically. Liu et al. [17] carried out a comparative study on a CFRP spoked wheel cable roof and a CFRP cable net facade numerically. They proved that Compared to steel cables, using CFRP cables in orthogonally loaded cable structures can significantly raise the structural stiffness if the amount of cable used is maintained. In addition, using CFRP cables can also considerably reduce the amount of cable used if the structural stiffness is maintained instead. Therefore, using CFRP cables in orthogonally loaded cable structures can improve the structural mechanical and economical performances.

Through numerical simulations, the foregoing studies have deepened the understanding on mechanical characteristics and failure mechanisms of CFRP spatial structures. But experimental studies are also needed to validate the results of theoretical studies and numerical simulations. Several tests on steel dome structures have been done. Chen et al. [18] designed a 1:10 steel suspended dome scale model, which was adopted in Chiping Stadium in China. Then, full-span and half-span loading tests were conducted to study the static performance of the structure. In order to study static mechanical properties of steel cable dome structures, two 6 m span dome structures were designed by Sun et al. [19]. One dome used steel tie rods as diagonal cables while the other used steel cables as diagonal cables. The static mechanical properties of the two cable domes under full-span and half-span load were compared by test. Zong and Guo [20] analyzed the static mechanical properties of a steel cable dome model with a diameter of 6 m under a vertical symmetrical and an antisymmetric loading. One 1:10 CFRP suspend dome scale model with a span of 4 m and a rise of 0.4 m was manufactured by Olofin and Liu [21] to evaluate the static performance for the imposed load on the single reticulated layer. Lu et al. [22] carried out a shaking table test on dynamic characteristics of a steel dome model using the white noise excitation method. The measured natural frequency and damping ratio were obtained and analyzed. The shaking table tests of single-layer reticulated steel dome are exploited to verify the failure pattern of the structure under seismic load records by Nie et al. [23].

Table 1
Details of the Load Cases.

Type of seismic wave	Maximum acceleration (gal)	Type of seismic wave	Maximum acceleration (gal)	Type of seismic wave	Maximum acceleration (gal)
Elcentro	100; 300; 500; 900	Kobe	50; 300; 500; 900	Pasadena	100; 170; 300; 500

However, few research papers have reported on seismic shaking table experiments for a CFRP cable dome structure. In addition, the joint details of a CFRP dome structure are different from that of a steel dome because of the great difference between the mechanical property of CFRP and that of steel. Therefore, improving the understanding of dynamic behavior of CFRP dome structures and finding a suitable joint form are very important when considering increasing the worldwide demands for such a kind of structure. To explore the dynamic performance of CFRP dome structures and find a joint form for practical engineering application, one shaking table test of a 1:22 scaled-down CFRP cable dome structure was conducted in this paper where the details of new joints and anchoring configurations were described. The seismic responses including the acceleration of joints, the member dynamic response of strain under the action of different seismic waves were analyzed and summarized. Meanwhile, a finite element model, which was identical with the test model, was established to carry out modal analysis.

2. Experimental program

2.1. Outline of the experiment

The test was completed on a seismic simulation shaking table of Southeast University in China. The shaking table has an effective load capacity of 30 tons and can produce a maximum horizontal movement of up to 3.0 g peak ground acceleration (PGA) when unloaded. Three kinds of seismic waves (Elcentro wave, Kobe wave and Pasadena wave) were selected to generate 12 load cases in the experiment (Table 1).

All seismic waves were horizontally input along one direction. In the shaking table test, the maximum acceleration of seismic waves needed to be adjusted to match the target acceleration of the above load cases, and the frequency of the waves needed to be adjusted according to the similarity ratio. The prototype of the dome structure had a diameter of 120 m and was scaled down at ratio of 1:22 in the experiment. The time duration of each seismic wave should be compressed to 1/22 of the recorded duration according to the similarity ratio. However, the duration of seismic waves would be too short to be loaded by the shaking table because the similarity ratio was too small. Therefore, the compression ratio of the seismic wave duration had to be appropriately increased and the duration of each seismic wave was adopted to be $1/\sqrt{10}$ of the original wave duration in the end. The acceleration time-histories of input wave that was compressed from recorded seismic waves is shown in Fig. 2. The uniformly distributed dead load was generally taken as $0.15kN/m^2$ and according to [EN 1991: Actions on structures], the uniformly distributed live load was $0.3kN/m^2$. The additional mass was applied by tying sandbags on the joints.

2.2. Details of the experimental model

Details of the test model are shown in Fig. 3. In the test, the fiber type was carbon fiber, the resin was epoxy resin and the fiber volume ratio was 0.6. One curved steel plate of 45 mm 33 mm was used as the internal

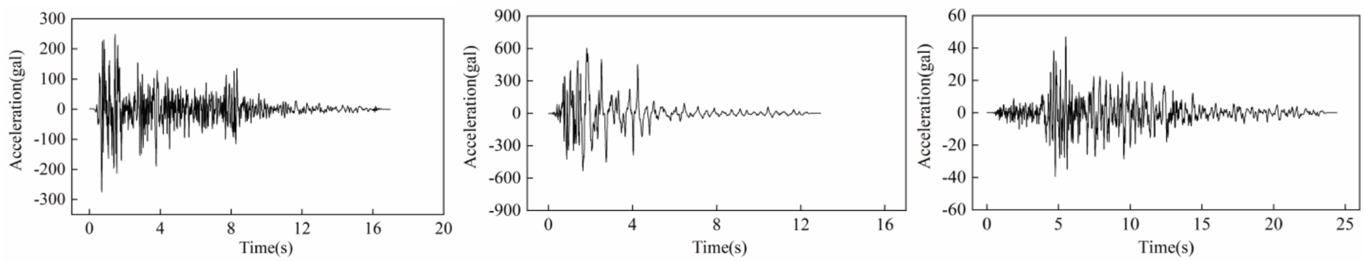

(a) Elcentro wave (b) Kobe wave (c)Pasadena wave

Fig. 2. Acceleration time-histories of input wave that was compressed from recorded seismic waves.

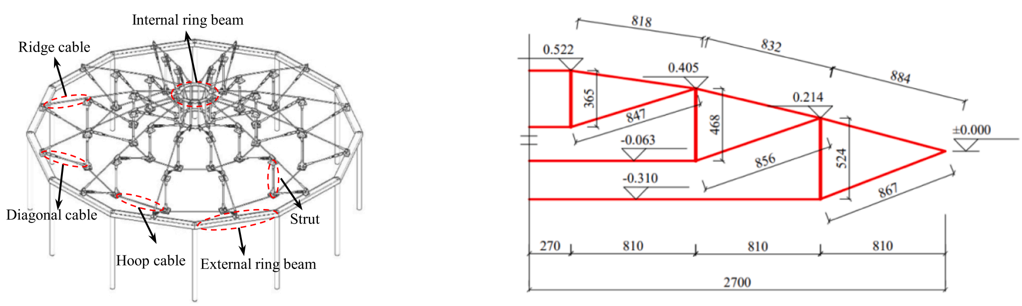

(a) Three-dimensional graph of the model (b) Elevation of the model (mm)

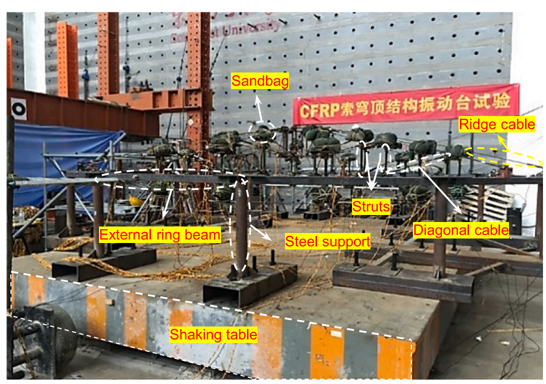

(c) The shaking table and model

Fig. 3. Details of the test model.

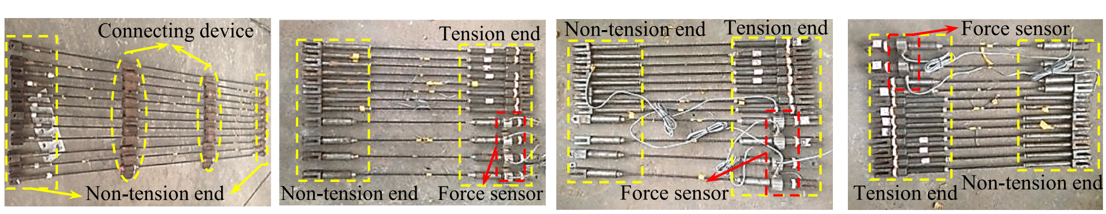

(a) Ridge cables (b) Outer diagonal cables (c) Middle diagonal cables (d) Internal diagonal cables

Fig. 4. The members of the model.

ring beam because the rotation radius of internal ring was too small for a CFRP bar to be curved. Middle hoop cables had a smaller radius of rotation than outer hoops. In order to make cables bend easily, CFRP bars with a smaller diameter were selected as middle hoop cables compared with outer hoop cables. Therefore, two parallel 5-mm-diameter CFRP bars and one CFRP bar with a diameter of 7 mm were used for middle hoop cables and outer hoop cables, respectively. Furthermore, in order to reduce the uneven distribution of internal force during tension and installation stages, the whole circle of a middle (outer) hoop cable was divided into two (three) segments. Single CFRP

Table 2
The mechanical properties of all the materials used.

Type of component	Material	Size (mm)	Elasticity modulus (MPa)	Ultimate tensile strength (MPa)
Internal ring beam	Steel	453 3	200,000	250
Middle hoop cables	CFRP	5	178,000	1432
The remaining cables	CFRP	7	178,000	1432
Outer and middle struts	CFRP	2032	96,000	1124
Internal struts	CFRP	1832	96,000	1124
External ring beam	Steel	14035.5380	200,000	250

bar with a diameter of 7 mm was used for each diagonal cable and one end of each diagonal cable could be tensioned [Fig. 4(b–d)]. Continuous CFRP bars with a diameter of 7 mm were selected as internal, middle and outer ridge cables. Different from diagonal cables, each ridge cable did not have tension ends [Fig. 4(a)]. In addition, the length of struts cannot be adjusted either. The elastic modulus and ultimate tensile strength of CFRP cables were 178,000 Mpa and 1432 Mpa, respectively. In the model, CFRP tubes with an outside diameter of 20 mm, a wall thickness of 2 mm and an elastic module of 96,000 Mpa were used for outer and middle struts while steel tubes with an outside diameter of 18 mm and a wall thickness of 2 mm were used for internal struts. The external ring beam was made of a steel channel with a height of 140 mm, a web thickness of 5.5 mm and a flange width of 80 mm. The mechanical properties of all the materials used are shown in Table 2.The joints connected to the external ring beam and internal ring beam adopted lugs to form hinges allowing these joints rotate freely in the vertical plane (Fig. 5).

The details of joints and anchoring methods of the CFRP dome were different from that of a steel cable dome for the mechanical properties of CFRP bars and steel strands were quite different. Because force sensors were installed on several diagonal cables, the anchorage length of these cables must be reduced. Therefore, a new type of tapered bonding anchorage with embedded steel ball was proposed in this study to connect ridge cables and force sensors [Fig. 6(a)]. The steel balls with different diameters can enhance the stiffness of gum resin. The cone shape can improve the grip effect of the tube. Both the balls in the resin and the cone shape of the tube can ensure the anchorage to obtain enough anchoring force with a shorter anchorage length compared with straight tube anchorages. Furthermore, compared with strand tapered anchorage for steel cables, this kind of anchorage can effectively avoid shear failure of CFRP bars caused by clamping. Traditional straight tube anchorages were applied in other cables. The anchorage lengths of new and traditional anchorages were 90 mm and 150 mm, respectively. The details of the upper and lower joints are shown in Fig. 6.

Forward and reverse threaded sleeves were used as tension devices in the test (Fig. 7). The outer and middle diagonal cables were selected as active tension cables and the rest cables were passive cables. Firstly, the length of passive cables was adjusted to be their original length, whose value equals to the length in the designed shape of dome minus the extension length value by prestressing. The length of active cables was slightly longer than their original length to ensure that the whole structure can be successfully installed. Then the active cables were tensioned step by step to their designed length, namely the cables' length in the designed shape of dome, whose value equals to the original length plus the extension length by prestressing. At the same time, the passive cables were also tensioned to their designed length. The initial prestress of members and the elevation of joints after the model being tensioned are shown in Tables 3 and 4.

2.3. *The Arrangement of measuring points*

The acceleration response of joints and dynamic response of strain were recorded during the experiment. A total of 16 accelerometers, 8 strain gauges and 1 linear variable differential transformer (LVDT) were set up in the test. The acceleration measuring points were represented by A1-16. Seven accelerometers (A1, A5–7 and A12–14) were arranged along the same direction as the movement of the shaking table (x-axis). Five accelerometers (A2, A3, A10, A11 and A15) were placed along the vertical direction. One accelerometer (A4) was arranged along y-axis, which is perpendicular to both x-axis and vertical plane. Moreover, three accelerometers (A8, A9 and A16) were set along the direction perpendicular to axis 3 or 5 in the horizontal plane. The strain gauges represented by S1–4 were used to measure the strain response of hoop cables, the gauges S5–6 and S7–8 were used to measure the strain response of diagonal and ridge cables, respectively. The LVDT was used to measure the horizontal displacement of the external ring beam to investigate whether the movement of the external ring beam was coordinated with that of the shaking table. One important thing must be mentioned that the measured displacement was that relative to the ground rather than to the shaking table, so the support of LVDT must be fixed to the ground. The numberings of each measuring point are shown in Fig. 8. The outermost numbers in Fig. 8 represent the axis numbering according to a counterclockwise order.

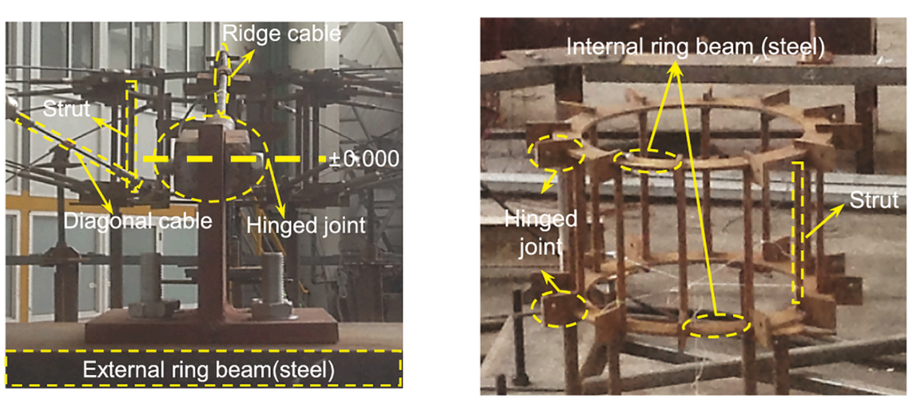

(a) Details of external ring beam joints (b) Internal ring beams and struts

Fig. 5. Details of external and internal ring beams.

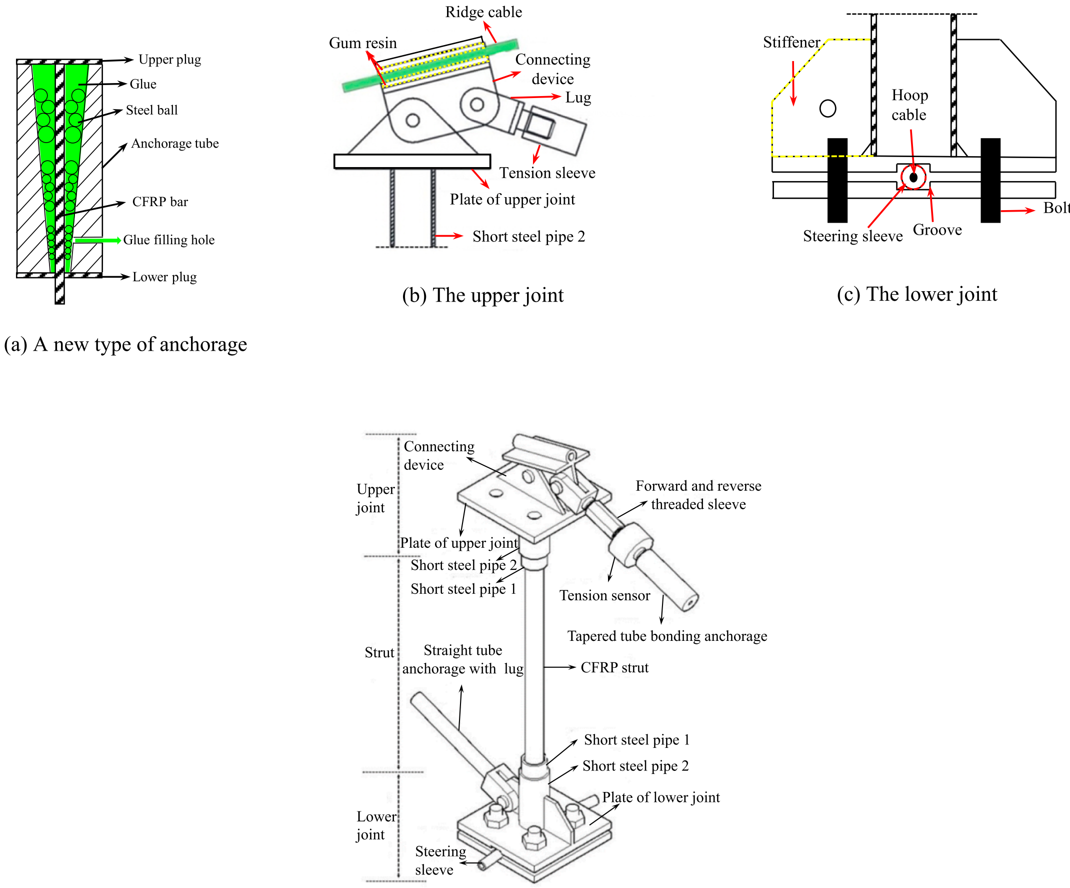

(a) A new type of anchorage (b) The upper joint (c) The lower joint

(d) A set of joints, struts, connecting devices and anchorage

Fig. 6. The upper and lower joints.

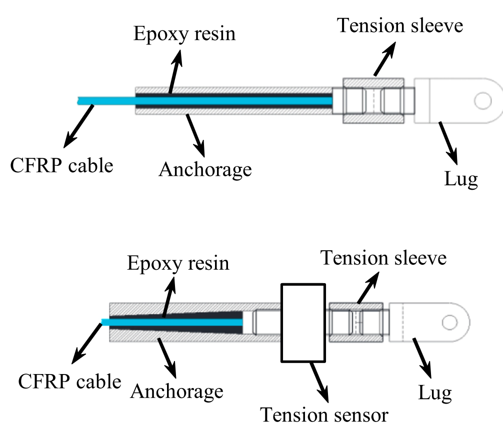

(a) Ordinary tensioning end (b) Tensioning end with tension sensor

Fig. 7. Pre-tension devices.

2.4. *Establishment of numerical model*

For an ordinary cable dome structure, the seismic response is influenced by the structural self-vibration characteristic. Therefore, to clearly describe the dynamic characteristics of the model, the finite element model identical to the test model was firstly analyzed by program ANSYS before discussing the test results (Fig. 9). Element types of Link8 and Link10 units adopt linear elastic material model to simulate the struts and cables, and the structural steel material of Ansys was used for the element type of Beam 188 to simulate the ring beams. In addition, Element type of Mass 21 was used to simulate the additional mass on the joints. The boundary conditions were fixed for the 12 outmost nodes, and the connection between the elements was realized by sharing nodes. The modal analysis in Ansys was used for the solution algorithm. The

Table 3
Initial Prestress of the model.

Member	Test value (N)	Theoretical value (N)	Error
Outer diagonal cable	2508	2774	−9.6%
Middle diagonal cable	1258	1388	−9.4%
Internal diagonal cable	472	425	11.1%
Outer ridge cable	1954	2386	−18.1%
Middle ridge cable	944	1021	−7.5%
Internal ridge cable	535	594	−9.9%
Outer hoop cable	4283	5004	−14.4%
Middle hoop cable	2097	2487	−15.7%

Note: The theoretical initial prestress of the model was calculated by singular value decomposition.

Table 4
Joint elevation of lower joints.

Joint	Designed elevation (cm)	Test elevation of joints (cm)				Average error
		Axis1	Axis 2	Axis 3	Axis 4	
Outer ring	−31	−32.3	−32.8	−31.2	−31.4	−1.40%
Middle ring	−6.3	−7.6	−7.4	−7.0	−7.6	−1.17%
Internal ring	15.7	16.2	16.5	15.9	16.2	0.42%

Note: The elevation ± 0.000 is aligned with the hinged joint above the external ring beam [Fig. 2(b) and 4(a)].

initial strain was applied into cables and struts to simulate prestress and the damping ratio of the model was taken as 0.02 According to Article 8.2.2 of Code for Seismic Design of Buildings (GB50011-2010).

3. Results and discussion

3.1. Natural frequency and structural vibration mode

According to numerical analysis results, the vibration modes are classified into the following categories: planar movement modes for upper joints [Fig. 10(a)], torsional movement modes for hoop cables [Fig. 10(b)] and vertical vibration modes (symmetric or anti-symmetric) [Fig. 10(c and d)]. Among the above modes, planar movement modes for upper joints and torsional movement modes for hoop cables occupy most of low order modes because the torsional stiffness of the Geiger type cable dome structure is small. The vertical vibration modes often occur in high order modes. Furthermore, most the vertical vibration modes are anti-symmetric. The first 100 orders of natural frequencies of the CFRP dome model are extracted and plotted in Fig. 11. The first natural vibration frequency of the model (planar movement modes for upper joints) is 1.159 Hz, and the natural frequency increases slowly with the vibration order. The reason is that the cable-dome structure is a complex structure, and its natural vibration modes are often the result of the coupling of adjacent modes. However, the finite element simulation results separate these coupled modes. Therefore, the natural vibration frequency of the cable-dome structure increases very slowly at the beginning, which is also the reason why the natural vibration frequency measured by the white noise method may miss part of the mode data. Only when the vibration order exceeds about 50, the natural frequency begins to rise rapidly with the order number because the natural vibration modes will become the overall vertical vibration and the coupling effect becomes small.

In the experiment, considering the limitation of experimental conditions, the white noise excitation method was used to measure the natural frequency of the structure. However, it was difficult to excite all the natural frequencies because the measurement accuracy of this method was not enough for measuring all the first 50 orders. The experimental and simulated results of several natural vibration

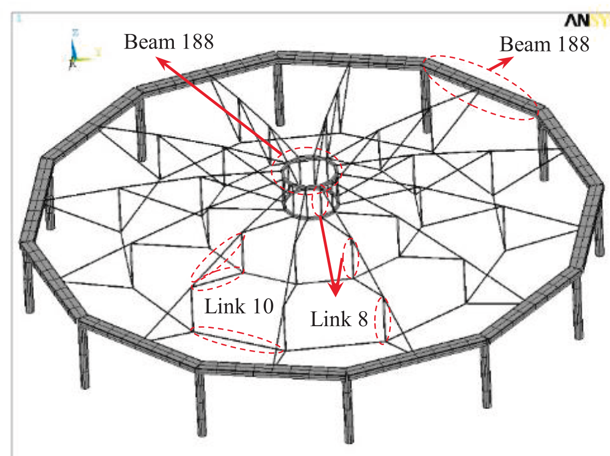

Fig. 9. Finite element model.

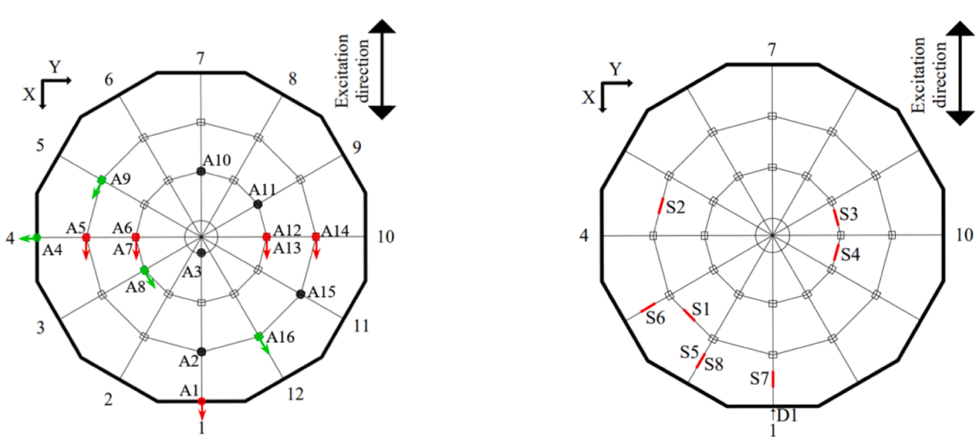

(a) Arrangement of accelerometers (b) Arrangement of strain gauges and LVDT

Fig. 8. Arrangement of measuring points. Note: The arrows in the figure indicate the measurement direction of accelerometers and LVDT. Moreover, acceleration sensors without arrow (A2, A3, A10, A11 and A15) indicate that those accelerometers measure the vertical direction acceleration.

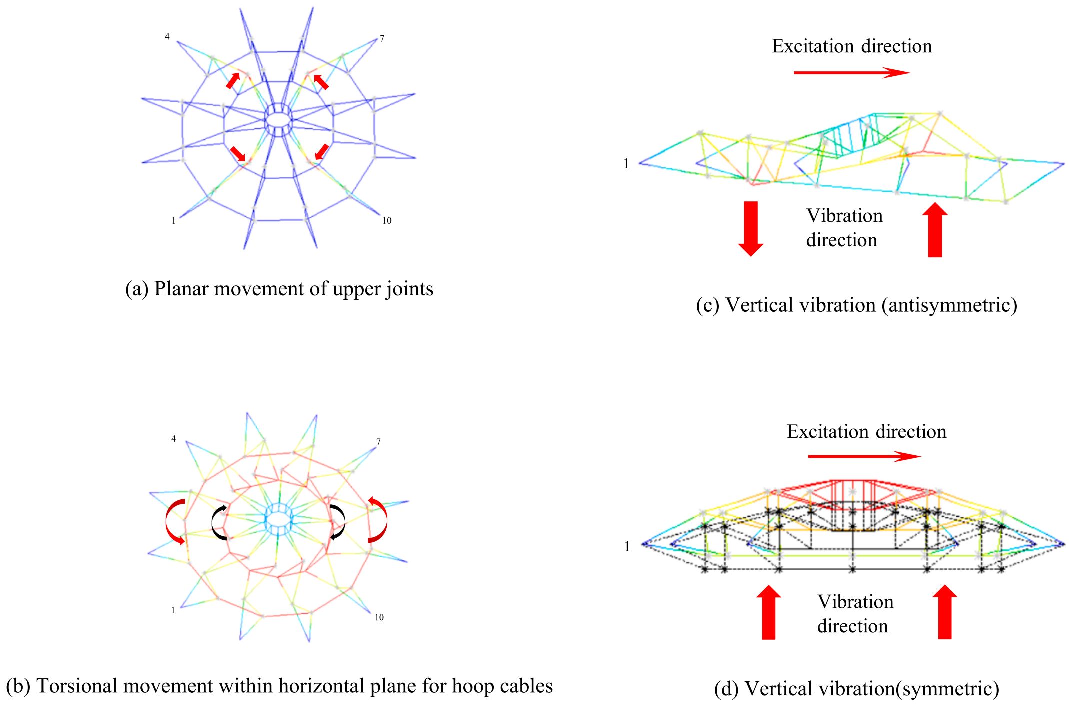

(a) Planar movement of upper joints

(c) Vertical vibration (antisymmetric)

(b) Torsional movement within horizontal plane for hoop cables

(d) Vertical vibration(symmetric)

Fig. 10. The vibration modes of the model.

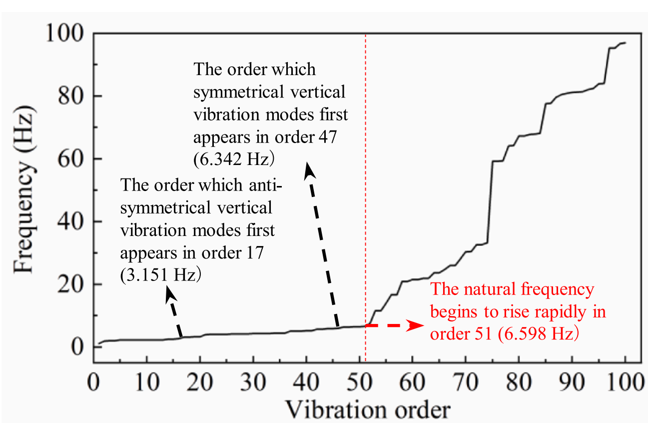

Fig. 11. Natural frequencies and vibration mode orders.

Table 5
Comparison between experimental and simulated results of natural vibration frequencies.

Order	Simulated results/Hz	Experimental results/Hz	Order	Simulated results/Hz	Experimental results/Hz
1	1.159	1.28	18	3.160	3.29
2	1.826	1.62	19	3.338	3.36
3	2.050	1.97	20	3.344	3.51
4	2.052	2.03	21	3.973	3.70
5	2.200	2.26	22	4.077	3.84
9	2.230	2.31	31	4.270	5.15
10	2.238	2.41	37	5.102	5.73
12	2.244	2.56	50	6.442	7.14
14	2.472	2.99	54	11.623	12.34

frequencies are shown in Table 5. The comparison results show that the results of numerical analysis are reliable.

3.2. *Analysis of experimental acceleration results under Elcentro wave*

Before analyzing the experimental data, it is necessary to mention that all joints and anchorages of the model were not damaged during the whole test, indicating that both the joint forms and the anchoring configurations in this study were reliable under the excitation test of strong seismic waves.

Firstly, E-wave (Elcentro wave), whose maximum acceleration was 249 Gal (0.254 g) for the original record, was selected for the test. The compressed time-history diagram of E-wave is shown in Fig. 2(a). E-Wave was tested for four load cases (E100, E300, E500 and E900). The number after the letter E indicates the maximum acceleration (gal) of the seismic wave in each case.

To discover response characteristics of joint vertical acceleration, the vertical responses of the outer-ring upper joint of axis 1 (A2, 1-OU-Z), the middle-ring upper joint of axis 7 (A10, 7-MU-Z) and the internal-ring lower joint of axis 1 (A3, 1-IL-Z) are selected for comparison (Fig. 12). The physical meaning for the numberings in the bracket is explained as follows. The first part represents the number [shown in Fig. 5(a)] of accelerometers. In the second part, the number represents the axis numbering, O represents outer ring while M and I are abbreviations for the middle ring and internal ring, respectively. U and L are abbreviations for upper joint and lower joint, respectively. The letter X, Y and Z represent the acceleration directions of the measuring points. For example, 1-OU-Z represents the vertical acceleration of the outer-ring upper joint of axis 1.

As shown in Figs. 9 and 10, the axes 1 and 7 are equivalent because they are symmetric with respect to the y-axis. As illustrated in Fig. 12, the CFRP dome structure follows the rule that on the same axis, the vertical acceleration response of middle-ring joints is the greatest and that of internal-ring joints is the lowest under the action of E-wave. The reason is that vertical vibration modes of the structure can be divided

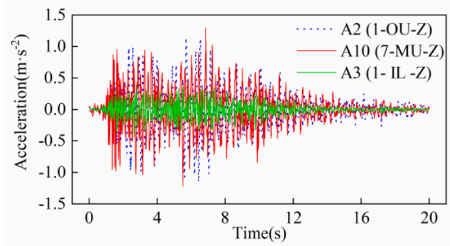

(a) Vertical acceleration under load case E100

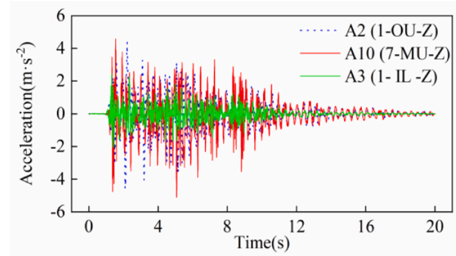

(c) Vertical acceleration under load case E500

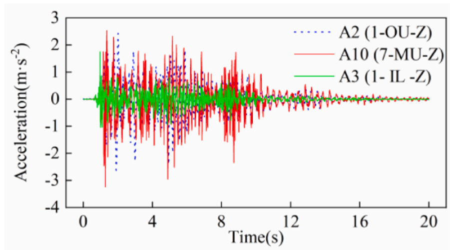

(b) Vertical acceleration under load case E300

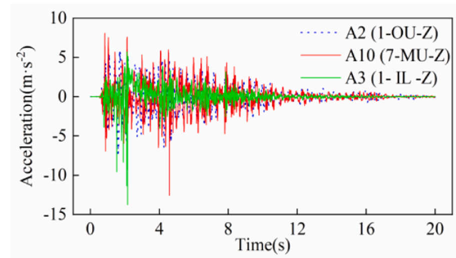

(d) Vertical acceleration under load case E900

Fig. 12. Comparison of vertical acceleration response of different joints.

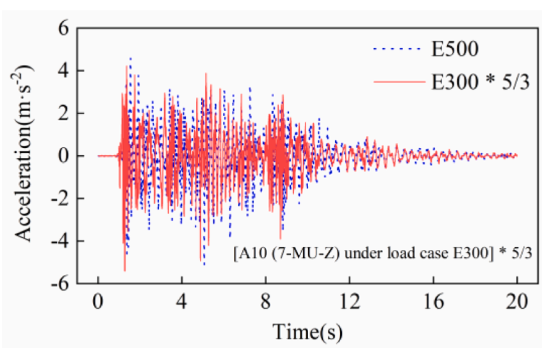

(a) [A10 (7-MU-Z) under load case E300] * 5/3

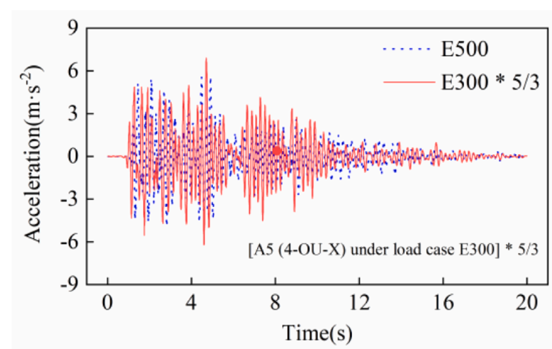

(b) [A5 (4-OU-X) under load case E300] * 5/3

Fig. 13. Comparison of acceleration time-histories of joints under the action of E-wave with different maximum acceleration.

into symmetrical vertical vibration modes [first appear in the 47th order, shown in Fig. 9(d) and 10] and anti-symmetrical vertical vibration modes [first appear in the 17th order, shown in Fig. 9(b) and 10]. In these two types of modes, anti-symmetrical vertical vibration mode is the lower order mode. In the anti-symmetric vertical vibration mode, the vertical acceleration of internal-ring joints is small because these joints are close to the center of the structure. Moreover, the vertical movement of outer-ring joints is small because outer-ring joints are closer to the external ring beam than middle-ring joints. Consequently, the vertical acceleration response of middle-ring joints is the greatest when vertical vibration modes are excited.

To explore the joint acceleration response rules under seismic waves of different maximum acceleration, the measuring points A10 (7-MU-Z) and A5 (4-OU-X) are selected for comparison because the z-direction and x-direction joint acceleration of these two joints is great. If the acceleration of joints under load case E300 is magnified by 5/3 times and then compared the curve (Fig. 13) with that under load case E500, the figure shows that the two curves basically agree with each other and the maximum value of the two curves is almost the same. Thus, the maximum response of acceleration increases basically linearly with the maximum acceleration of the input seismic wave.

For a Geiger-type cable dome, the lower joints are constrained by hoop cables while the upper joints lack transverse constraints. To investigate whether the transverse connection can reduce the acceleration response of joints, the measuring points A6 (4-MU-X) and A7 (4-ML-X) are selected for comparison (Fig. 14). It appears that the maximum acceleration of A6 (located at upper joint) is obviously greater than that of A7 (located at lower joint) under load cases E100 to E900. Therefore, the transverse connection between joints effectively reduced the joint acceleration response. In addition, it is conspicuous that the x-direction acceleration of A6 is greater than that of A5. Because the distance between the outer ring and the external ring beam is closer than the distance between the middle ring and the external ring beam (Fig. 15). The constraint of the rigid external ring beam on the outer ring is greater than that on the middle ring.

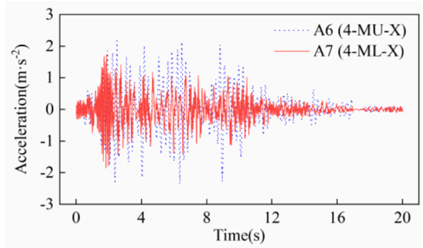

(a) X-direction acceleration under load case E100

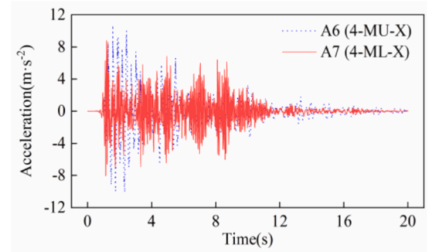

(c) X-direction acceleration under load case E500

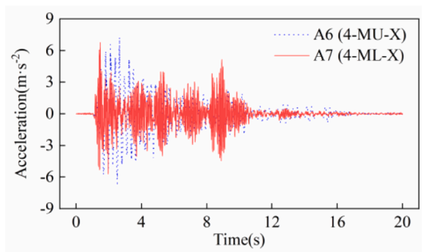

(b) X-direction acceleration under load case E300

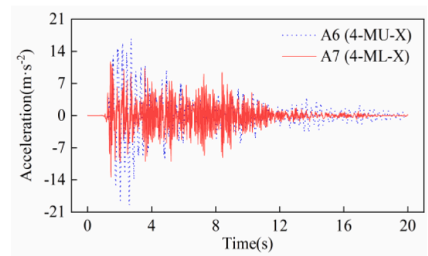

(d) X-direction acceleration under load case E900

Fig. 14. Comparison of x-direction acceleration responses between measuring points A6 and A7 under different load cases.

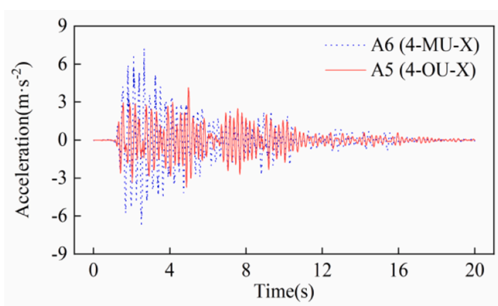

(a) X-direction acceleration under load case E300

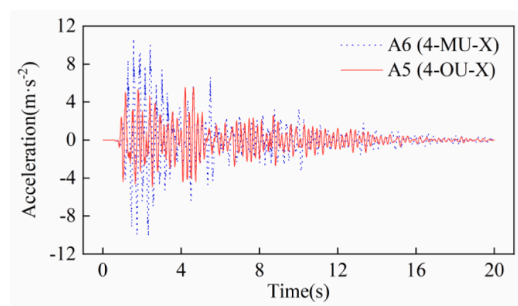

(b) X-direction acceleration under load case E500

Fig. 15. Comparison of x-direction acceleration responses between measuring points A5 and A6 under different load cases.

3.3. Analysis of experimental strain results under Elcentro wave

Fig. 16 shows dynamic time-history responses of strain for outer and middle ring cables under load case E300, for the initial prestress force of these members are large. The dynamic response of strain refers to the difference between the strain produced under the action of seismic waves and the initial strain produced by the prestressing of the model. In Fig. 15, the strain whose values less than 0 means the initial prestress of cables is reduced during the whole excitation process. Meanwhile, the maximum amplitude for dynamic response of strain under different load cases are compared in Fig. 16. As shown in Figs. 16 and 17, the dynamic response of strain meets the following rule: outer hoop cables > outer ridge cables > middle hoop cables > outer diagonal cables. In addition, the maximum amplitude for dynamic response of strain increases basically linearly when the maximum acceleration of seismic wave increases.

3.4. Analysis of experimental acceleration results under Kobe wave and Pasadena wave

The near-field earthquake is characterized by higher energy impulsion motion, more low frequency components and larger acceleration amplitude compared with E-wave, which makes a structure directly bear high energy impact. The long duration seismic wave means that the structure withstands cyclic loads for a longer period compared with E-wave, which makes a dome structure produce a greater displacement response because the stiffness of dome structures is small. Therefore, these two types of earthquakes may cause the model to produce a greater dynamic response. In the test, the near-field K-wave (Kobe wave) recorded by the Hanshin earthquake in Japan and the long duration P-wave (Pasadena wave) recorded by the California earthquake in the United States were selected for the test. The maximum accelerations of these two recorded seismic waves were 0.617 g (604.7 Gal) and 0.0478 g (46.8 Gal), respectively. The compressed time-history diagrams of these two seismic waves are shown in [Fig. 2(b) and (c)]. K-wave and P-wave were tested in four load cases, respectively (K50, K300, K500, K900, P100, P170, P300 and P500). The acceleration time-history curves of measuring points along z-direction and x-direction under the action of K300 and P300 are shown in Fig. 18. From the figures, the CFRP dome structure still meets the rule that vertical acceleration of middle-ring joints is the greatest among all rings. Moreover, x-direction acceleration of upper joints is larger compared with lower joints.

The maximum amplitude of joint acceleration under the action of different seismic waves are compared in Fig. 19. As shown in Fig. 19, the

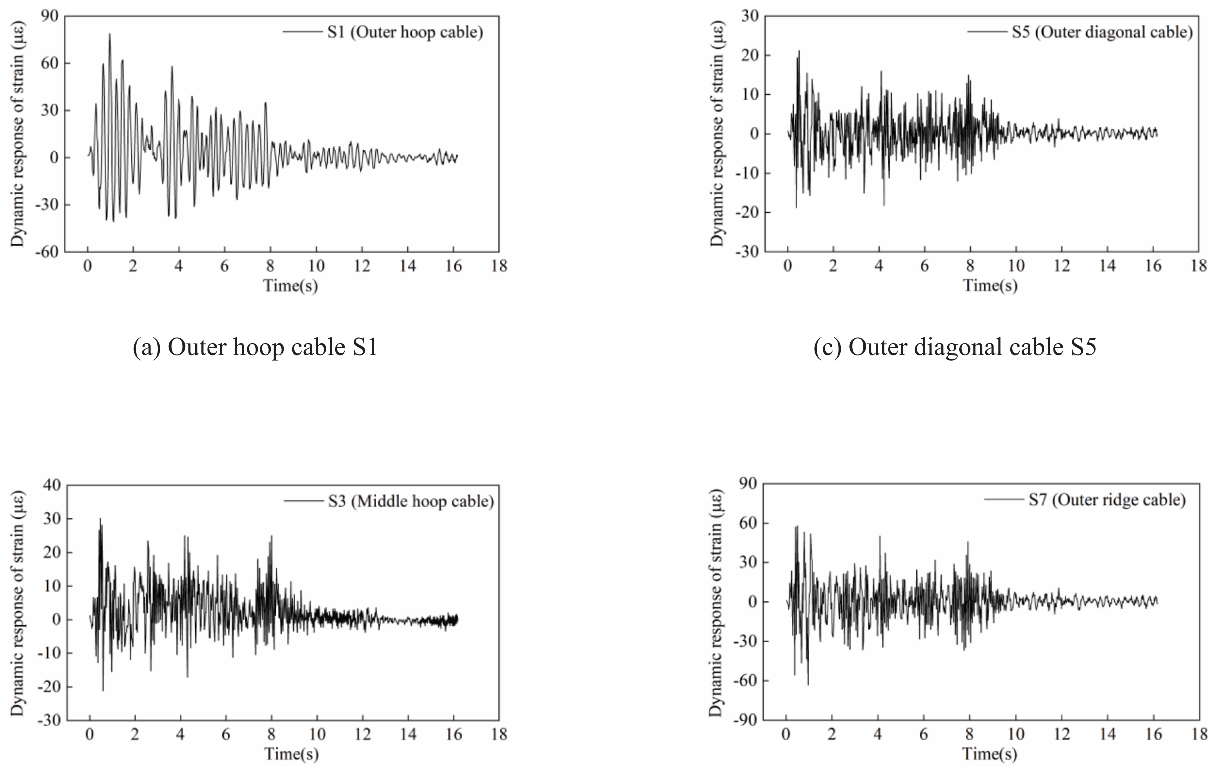

(a) Outer hoop cable S1

(c) Outer diagonal cable S5

(b) Middle hoop cable S3

(d) Outer ridge cable S7

Fig. 16. Strain responses of different elements under load case E300.

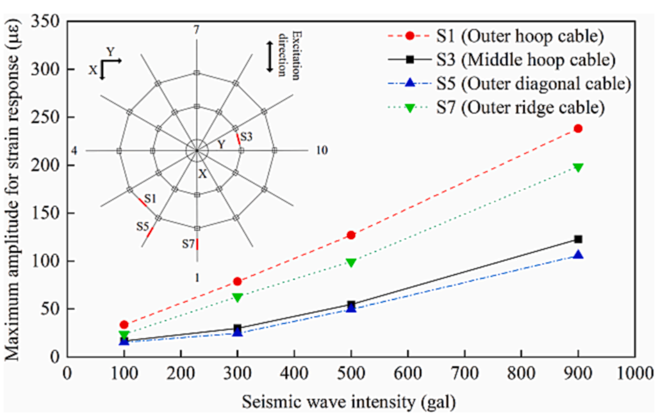

Fig. 17. Maximum amplitude for strain response under different E-wave load cases.

acceleration response of the structure caused by P-wave is the strongest and that caused by E-wave is the smallest. To explain this phenomenon and compare the spectrum feature of these waves, fast Fourier transform (FFT) is used to transform time-history curves of seismic waves into frequency spectrum (Fig. 20). It can be seen from Fig. 20 that E-wave amplitude of high frequency part is greater compared with that of the other two seismic waves, and the frequency region with high amplitude of P-wave is wider than that of K-wave. Moreover, the maximum amplitude of K-wave is the greatest among those three seismic waves. Generally, structures under the action of seismic waves are mainly controlled by low order modes which require less energy. As illustrated in Fig. 11, the frequencies of the first 16 orders are all below 3 Hz. Because the Fourier amplitude of E-wave between 1 Hz and 3 Hz is the smallest among the three types of waves, E-wave causes the smallest acceleration response of the dome structure. In addition, the frequencies of P-wave with high Fourier amplitude are distributed within the region between 2 Hz and 7 Hz. This region can excite the first 50 modes (shown in Fig. 11), resulting in the greatest acceleration response. Compared with the other two seismic waves, the frequency region with high amplitude of K-wave is the narrowest though the maximum amplitude of K-wave is the greatest. Therefore, the acceleration response caused by K-wave is smaller than that caused by P-wave.

3.5. Analysis of experimental strain results under Kobe wave and Pasadena wave

Fig. 21 shows maximum amplitude for dynamic response of strain under the action of K-wave and P-wave. As can be seen from the figure, the maximum strain response of members still meets the rule that outer hoop cables > outer ridge cables > middle hoop cables > outer diagonal cables.

4. Conclusion

To study the dynamic response of a CFRP cable dome structure under different seismic waves, this study carried out a shaking table experimental research and numerical simulations on the dynamic behavior of a Geiger-type CFRP cable dome scale model with a diameter of 5.4 m. The main conclusions are as follows:

1. New types of joint forms and anchoring configurations for the CFRP cable dome models are proposed because the existing forms for steel domes cannot be applied to CFRP dome structures. It has been proved by the shaking table experiment that the new types of joint forms and anchoring configurations are reliable under strong seismic waves.

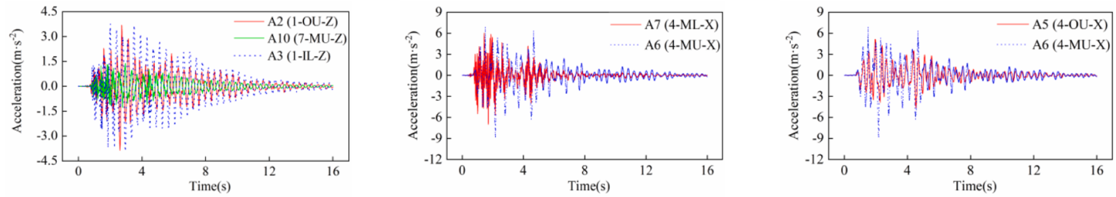

(a) A2, A3 and A10 under load case K300 (c) A6 and A7 under load case K300 (e) A5 and A6 under load case K300

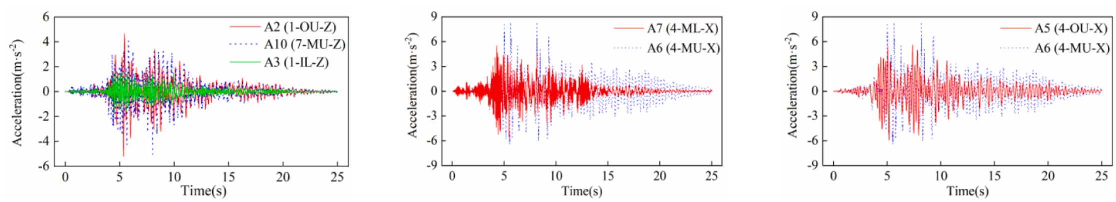

(b) A2, A3 and A10 under load case P300 (d) A6 and A7 under load case P300 (f) A5 and A6 under load case P300

Fig. 18. Comparison of joint acceleration responses under K-wave, P-wave.

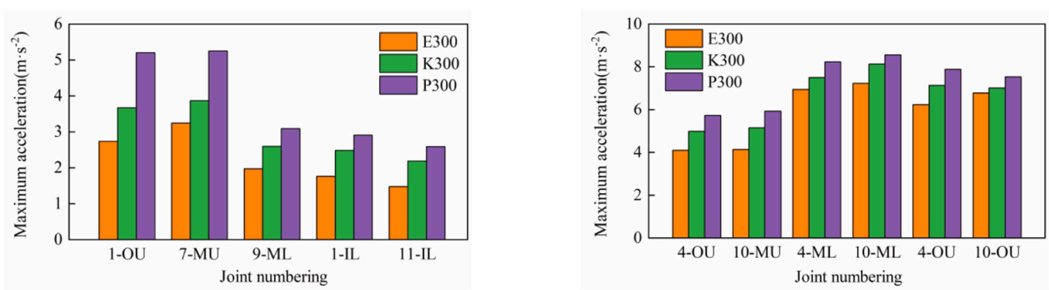

(a) Maximum vertical acceleration (b) Maximum x-direction acceleration

Fig. 19. Comparison of maximum acceleration under different seismic waves.

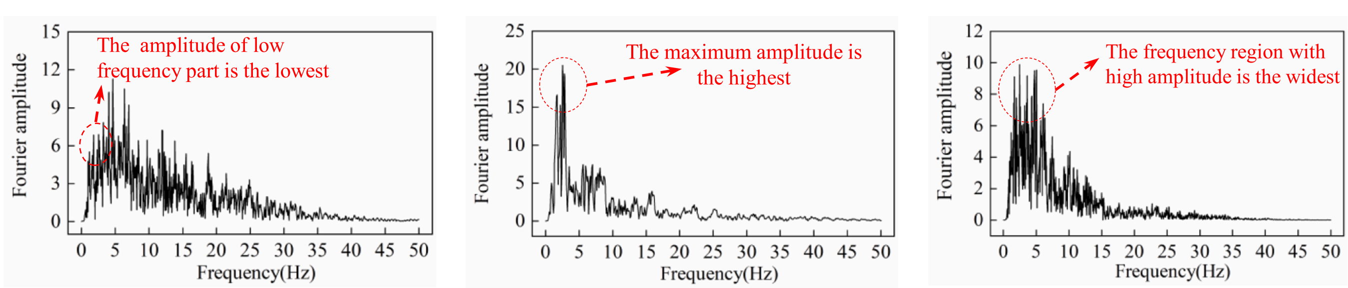

(a) Frequency spectrum of E300 (b) Frequency spectrum of K300 (c) Frequency spectrum of P300

Fig. 20. Frequency spectrum diagram of different seismic waves.

2. The vibration modes with large mass participation coefficient are vertical modes for CFRP dome structures. Among these vertical vibration modes, control modes are anti-symmetrical vertical modes because the frequencies of these modes are lower than those of symmetrical vertical modes. Therefore, the middle-ring joints have larger vertical acceleration than outer ring and internal ring joints. The acceleration response of structure can be reduced by setting stays on the middle ring joints in practical engineering.
3. Upper joints have larger transverse direction acceleration compared with lower joints because the lower joint is connected by hoops. Transverse connection between joints can effectively reduce the joint acceleration response. Therefore, the joints acceleration response can be reduced by placing purlins or stays between the upper joints in practical engineering.
4. Dynamic response of cable dome structures is closely related to the spectrum characteristics of seismic waves. The stiffness of the Geiger-type CFRP dome structure is small. Therefore, the Pasadena wave,

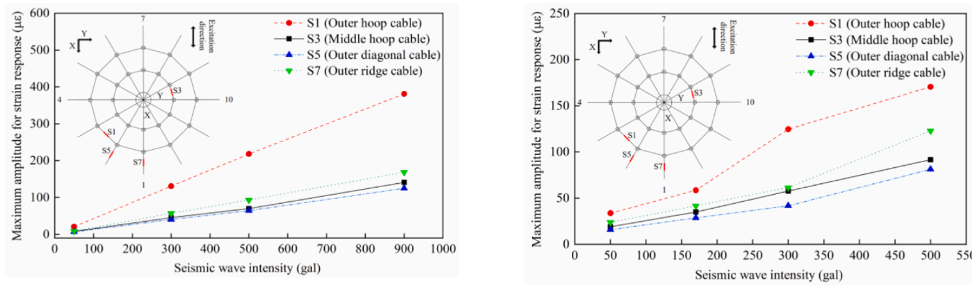

(a) Maximum amplitude for strain response under different K-wave load cases

(b) Maximum amplitude for strain response under different P-wave load cases

Fig. 21. Maximum amplitude for dynamic response of strain under K-wave, P-wave.

which has a wide low frequency region for high Fourier amplitude, can excite the greatest acceleration response. In practical engineering, different structural forms can be adopted for different areas to avoid resonance with frequent local earthquakes.

Declaration of Competing Interest

The authors declare that they have no known competing financial interests or personal relationships that could have appeared to influence the work reported in this paper.

Data availability

Data will be made available on request.

Acknowledgments

This work was supported by the National Natural Science Foundation of China [grant numbers 51378108, 51678137]; the Fundamental Research Funds for the Central Universities [grant numbers 2242022k30031, 2242022k30033].

References

[1] Guo JM, et al. Control equation of feasible pre-stresses and feasibility of new types of rotating surface cable domes. Eng Struct 2021;246:113000. https://doi.org/10.1016/j.engstruct.2-021.113000.
[2] Kawaguchi M, Tatemichi I, Chen PS. Optimum shapes of a cable dome structure. Eng Struct 1999;21(8):719–25. https://doi.org/10.1016/S0141-0296(98)00026-1.
[3] Krishnan S. Structural design and behavior of prestressed cable domes. Eng Struct 2020;209:110294. https://doi.org/10.1016/j.engstruct.2020.110294.
[4] Wang YF, Xu X, Luo YZ. Minimal mass design of active tensegrity structures. Eng Struct 2021;234:111965. https://doi.org/10.1016/j.engstruct.2021.111965.
[5] Siwowski T, Piątek B, Siwowska P, Wiater A. Development and implementation of CFRP post-tensioning system for bridge strengthening. Eng Struct 2015;207:110266. https://doi.org/10.1016/j.engstruct.2020.110266.
[6] Meier U. Proposal for a carbon fiber reinforced composite bridge across the strait of Gibraltar at its narrowest site. SAGE Open 1987;201(22):73–8. https://doi.org/10.1243/PIME_PROC-_1987_201_048_02.
[7] Shahawy M, Beitelman TE. Static and fatigue performance of RC beams strengthened with CFRP laminates. J Struct Eng 1999;125(6):613–21. https://doi.org/10.1061/(ASCE)0733-9445(1999)125:6(613).
[8] Zou PXW. Long-term properties and transfer length of fiber-reinforced polymers. J Compos Constr 7(1), 10–19. https://doi.org./10.1061/%28ASCE%2910900268%282003%-297%3A1%2-810%29.
[9] Sleeper B, Arnold S, Pridmore A, Carr H. Carbon Fiber Reinforced Polymer (CFRP) As a Long Term Repair Solution. Rep., Pipeline Division Specialty Conference., Keystone, Colorado, United States; 2010. https://doi.org/10.1061/41138(386)108.
[10] Wang X, Wu ZS. Evaluation of FRP and hybrid FRP cables for super long-span cable-stayed bridges. Compos Struct 2010;92(10):2582–90. https://doi.org/10.1016/j.co-mpstruct.2-010.01.023.
[11] Wen X, Cai CS, Zhang Y, Xiao RC. Study of super long span cable-stayed bridges with CFRP components. Eng Struct 2011;33(2):330–43. https://doi.org/10.1016/j.engst-ruct.2010.10.013.
[12] Yang YQ, Wang X, Wu ZS. Evaluation of the static and dynamic behaviors of long-span suspension bridges with FRP cables. J Bridg Eng 2016;21(12):06016008. https://doi.org/10.1061/(ASCE)BE.1943-5592.0000972.
[13] Liu MH, Qiang SZ, Xu GP, Ren WP. Study and prototype design of a suspension bridge with ultra-long span and CFRP main cables. J. Highw. Transp. Res. Dev. (English Edition) 2014;8(4):47–56. https://doi.org/10.1061/JHTRCQ.0000410.
[14] Flaga K. Advances in materials applied in civil engineering. J Mater Process Technol 2000;106(1–3):173–83. https://doi.org/10.1016/S0924-0136(00)00611-7.
[15] Lu ZT, Mei KH. First application of CFRP cables for a cable-stayed bridge in China. China Civil Eng. J. 2007;40(1):6. in Chinese.
[16] Serdjuks D, Rocens K, Pakrastinsh L. Utilization of composite materials in saddle-shaped cable roofs. Mech Compos Mater 2000;36(5):385–8. https://doi.org/10.1023/A:1026-647117370.
[17] Liu Y, Zwingmann B, Schlaich M. Advantages of using CFRP cables in orthogonally loaded cable structures. AIMS Mater Sci. 2016;3(3):862–80. https://doi.org/10.3934/maters-ci.2016.3.862.
[18] Chen ZH, Yan RZ, Wang XD, Liu HB, Xiao X. Experimental researches of a suspen-dome structure with rolling cable-strut joints. Adv Steel Constr 2015;11(1):15–38. https://doi.org/10.18057/IJASC.2015.11.1.2.
[19] Sun GJ, Xiao S, Xue SD. Test and numerical investigation mechanical behavior of cable dome. Int J Steel Struct 2021;21(6):1502–14. https://doi.org/10.1007/s13296-021-00517-7.
[20] Zong ZL, Guo ZX. Experimental research on mechanical properties and cable broken of levy cable dome. Eng. Mech. 2013;30(1):271–6. in Chinese.
[21] Olofin IO, Liu R. Research on the static behaviour of a suspen dome with carbon fibre reinforced polymer (CFRP) tensegrity system. IJST-T Civ Eng 2020;3:1–19. https://doi.org/10.1007/s40996-020-00488-5.
[22] Lu Z, et al. Shaking table experimental and numerical investigations on dynamic characteristics of suspend-dome structure. Structures 2022;40:138–48. https://doi.org/10.1016/j.ist-ruc.2022.04.001.
[23] Nie GB, Zhi XD, Fan F, Dai JW. Failure pattern of singe-layer reticulated dome under severe earthquake and its shaking table test. Int J Steel Struct 2014;14:399–409. https://doi.org/10.1007/s13296-014-2018-9.